Hydrogen storage capacity of submicron magnesium–nickel alloys

R. L. HOLTZ
Geo-Centers, Inc., 10903 Indian Head Highway, Fort Washington, MD 20744, USA

M. A. IMAM
Materials Science and Technology Division, Code 6323, US Naval Research Laboratory, Washington, DC 20375, USA

Magnesium–nickel alloys with nickel concentrations from 0 to 60 at % were prepared by three methods: inert gas condensation of sputtered nanocrystalline powder, cosputtering of amorphous thin films and ball milling. Of the three methods, ball milling yields the best hydrogen storage properties in terms of hydrogen capacity, hydriding/dehydriding rates, and activation requirements. In addition, these characteristics are achieved in magnesium with only very small nickel concentrations, on the order of a few atomic per cent.

1. Introduction

Magnesium–nickel alloys are potential candidate materials for practical hydrogen storage systems [1, 2]. Pure magnesium has a hydrogen capacity of 7.6 wt %, in the form of the MgH_2 compound, the highest capacity of any solid hydride except LiH. However, pure magnesium is prone to oxide "poisoning", which reduces the rates of hydriding and dehydriding. In addition, the hydrogen desorption temperature, 290 °C, is marginal for prospective applications. The alloy Mg_2Ni is more stable in air, with an attractive hydrogen desorption temperature of 250 °C, but lower hydrogen capacity of 3.6 wt %. In the context of hydrogen storage, Mg_2Ni is the composition that has received the most attention.

Due to the large difference in melting temperatures and the high vapour pressure of magnesium, it is difficult to make magnesium–nickel alloys by melt processing. A demonstrably better method is mechanical alloying, or ball-milling, which has been used to produce Mg_2Ni with respectable hydrogen storage characteristics and better properties than ingot-prepared alloy [3, 4]. The hydrogen storage capacity reported was 90% or less of theoretical values, and these materials require a number of hydride–dehydride cycles for activation.

High-energy ball milling has been used to produce Mg_2Ni with particle sizes in the range of 20 to 30 nm [5] and more recently as small as 4 nm [6]. The smaller grain sizes enhance the hydrogenation and dehydrogenation rates, lower the absorption temperatures and reduce the activation treatments needed. Another important aspect is that incorporating traces of palladium with the Mg_2Ni further enhances the hydriding characteristics, even allowing room temperature hydrogen absorption and eliminating the need for activation entirely [7]. It was argued in that report that dispersed palladium particles in contact with the Mg_2Ni altered the surface catalytic activity of the material to produce these effects.

It is desirable to reduce the nickel concentration to increase the hydrogen capacity. Some work has been reported on magnesium alloys with as low as 4 at %, prepared by ingot metallurgy and subsequently crushed to 40 mesh powder [8, 9]. These alloys have been shown to be suitable for hydrogen storage, although smaller particles and even lower nickel content would be better. Recently, mechanically alloyed magnesium with as low as 2 at % nickel has been reported [10, 11] to have high hydrogen capacities, high hydriding and dehydriding rates, and easy activation.

An older body of work exists concerning magnesium with small percentages of dispersed nickel particles [12,13] prepared by chemical vapour methods. Those results suggest that hydrogen storage characteristics can be enhanced via the catalytic action of dispersed nickel in magnesium in a manner similar to the dispersed palladium in Mg_2Ni noted above.

The confluence of the various results described above represents the thrusts of the work reported here: synthesis of magnesium–nickel alloys with the low nickel concentration as the storage material, with fine particle sizes in the submicron or nanocrystalline regime to enhance the kinetics. Three methods of synthesizing magnesium–nickel alloys were used: (i) physical vapour deposition with inert gas condensation, (ii) decomposition or pulverization by hydride–dehydride cycling of thin films, and (iii) ball milling. The desired particle size and composition ranges were easily achieved by ball milling.

2. Materials synthesis and processing

Three synthesis methods were used: inert gas condensation synthesis of nanocrystalline powder, co-deposition of amorphous thin films and ball milling. Fig. 1

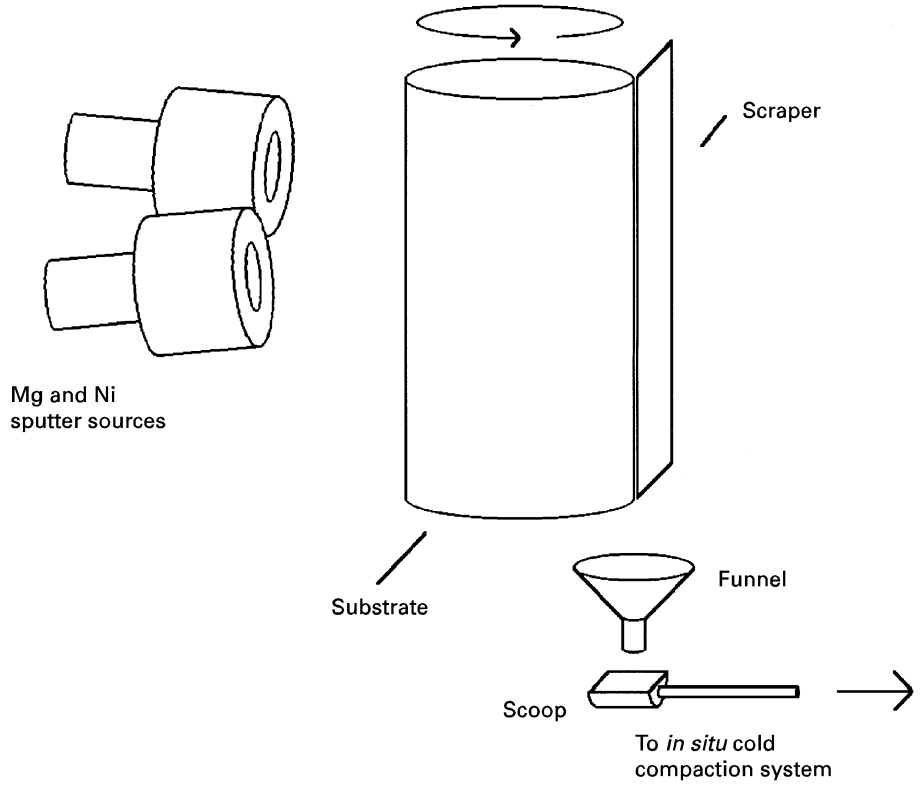

Figure 1 Depiction of the physical vapour deposition inert gas condensation (PVD/IGC) system used to prepare nanocrystalline and amorphous thin film magnesium–nickel specimens.

depicts the essential elements of the inert gas condensation method of producing nanocrystalline metals. Metals are sputtered or evaporated into an atmosphere of argon, where they condense into small particles and are transported via thermal convection to the rotating liquid-nitrogen cooled substrate surface. Following deposition, the substrate is scraped and the material collected. It is then transported *in situ* in high vacuum to a uniaxial cold press where it is formed into small pellets. This is a standard technique and is described in the literature on nanostructured materials over the past several years, and the particular deposition system used in the present work is described elsewhere [14]. To synthesize the nanocrystalline magnesium–nickel alloys, a composite split sputtering target of magnesium and nickel, (40% Ni by area or 76% by weight) was sputtered at 250 W in an atmosphere of 20 Pa of argon for 2 h. This yielded approximately 8 mg of nanocrystalline magnesium–nickel alloy powder with a nickel concentration of 50 at %, estimated from the weight losses from the sputtering target and energy dispersive spectrometry. The material was then pressed at 500 MPa into a pellet of 6 mm diameter. Only a few specimens were made before the method was abandoned as impractical for making pellets large enough to reliably measure the hydriding properties.

By reducing the argon pressure during deposition to 2 Pa, using the same deposition system and procedures, thin films rather than nanocrystalline powders are obtained. For this work, a series of magnesium–nickel films were deposited from separate magnesium and nickel sputtering targets. Specimens with concentrations of 0, 15, 33, 60, 85 and 100 at% were made. Compositions were changed by using different sputtering powers, which ranged from 50 to 500 W for each source, depending on the concentration obtained. Typical deposition rates of 2–4 mm h^{-1} were obtained, yielding pellets of 0.1 to 0.5 g, 6.4 mm diameter and 0.5 to 2 mm thick. Except for the pure magnesium, the as-deposited films were amorphous. All of the films had a typical columnar thin film microstructure. When scraped from the substrate and compacted, the pellets consist of compacts of small, broken flakes of these films. A more detailed description of these experiments and the results is available elsewhere [15].

Ball-milled materials were prepared by milling up to 750 cm^3 of magnesium and nickel powders immersed in commercial grade mineral oil, in an attritor, Union Process ball mill. Starting magnesium and nickel powders were -20 $+100$ and -100 mesh, respectively. The total milling time of 50 h was chosen because it optimized the particle sizes obtained. This method produced grain size refinement to less than 100 nm for a composition of 33% nickel. Subsequently, the same milling time was used for all of the specimens, and this time was not optimized further. Following milling, the bulk of the mineral oil was drained by allowing the milled material to settle in a beaker followed by pouring off the excess mineral oil. The material obtained was still damp with some oil. Portions of the material were uniaxially cold pressed in air at 900 MPa. The pellets were 9.5 mm diameter and several millimetres thick, with a mass of approximately 1 g each. Pressing squeezed out several

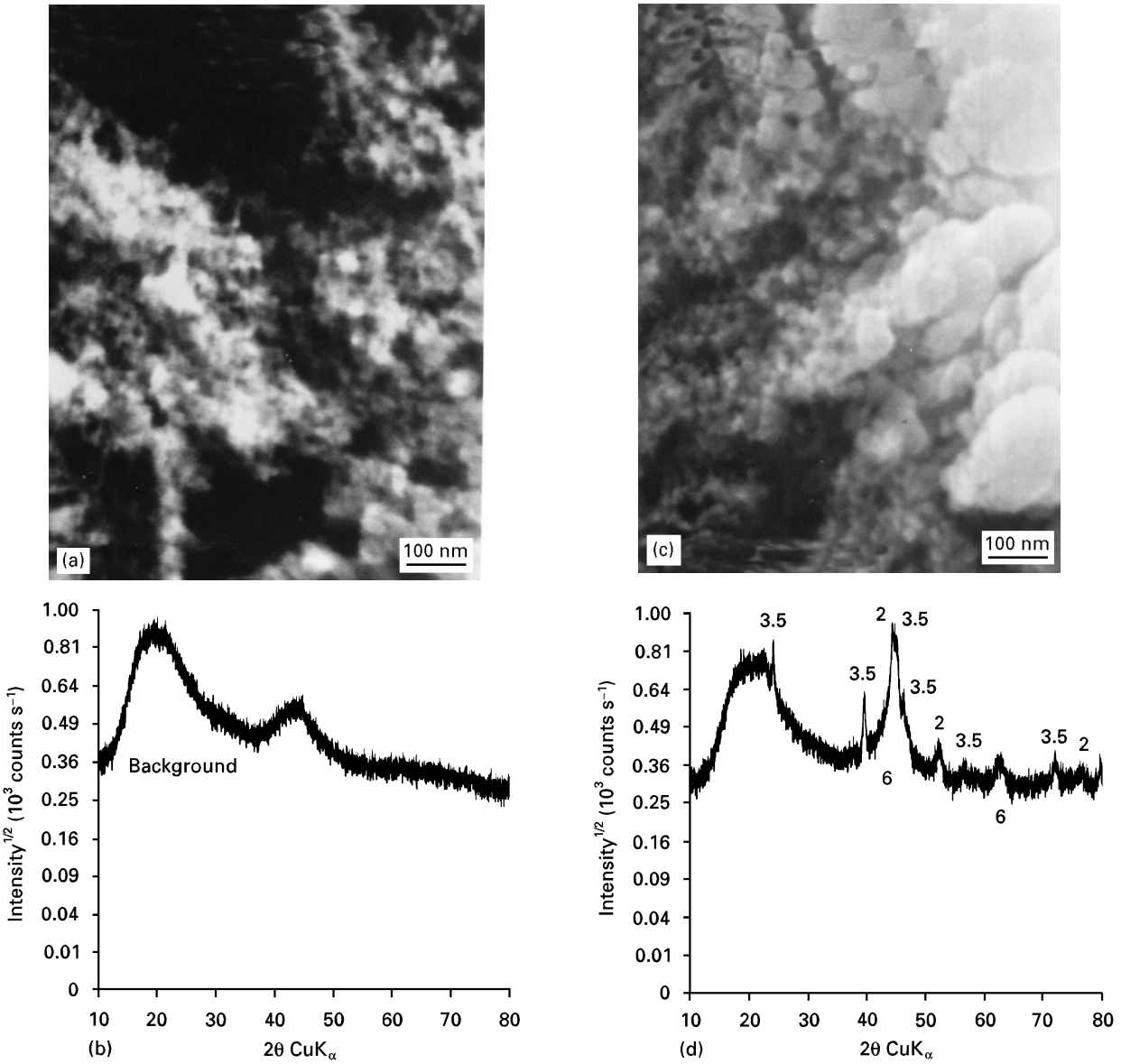

Figure 2 Microstructure and X-ray diffraction patterns of (a) and (b) as-prepared and (c) and (d) hydrided nanocrystalline magnesium–nickel prepared by sputtering/inert gas condensation with approximately 50 at % nickel (hydrided at 350 °C and 2 MPa). Key: 1, Mg; 2, Ni; 3, Mg_2Ni; 4, MgH_2; 5, Mg_2NiH_4; 6, MgO.

drops of mineral oil from the material and consolidated it without exposure to air. Consolidated densities relative to theoretical density ranged from 77% for specimens with higher nickel content to 97% for pure magnesium. Specimens with varying nickel concentrations of 0, 0.1, 1, 2.5, 5, 10, 20, and 33 at % were made.

The apparatus used for hydriding and dehydriding the specimens consisted, essentially, of a seamless stainless steel tube reaction chamber with metal gasket seals, sitting in a tube furnace. All hydriding treatments were performed at 350 °C and 2 MPa hydrogen pressure. Dehydrogenation was performed at the same temperature in a rough vacuum of a few Pa pressure. Initially, the hydrogen uptake of the specimens was determined by removing the specimens from the chamber between each hydride–dehydride cycle and weighing them. This was found to be unsatisfactory due to irreversible weight gains due to oxidation when the specimens were exposed to air. Subsequently, the balance and the access end of the reaction tube were enclosed in an argon-filled glove bag, which reduced the oxidation problem, but not entirely [15]. For the ball-milled specimens, which were larger than the film or nanocrystalline specimens, it was possible to measure the hydrogen capacity by measuring the pressure changes in the reaction chamber at room temperature before and after a hydride or dehydride treatment. This pressure change method was found to yield essentially the same results as the reversible part of the weight changes.

3. Microstructure changes with hydriding

Scanning electron micrographs and X-ray diffractometer scans are shown in Figs 2, 3 and 4 for representative specimens of the as-prepared and hydrided material prepared by inert gas condensation, thin film deposition and ball milling.

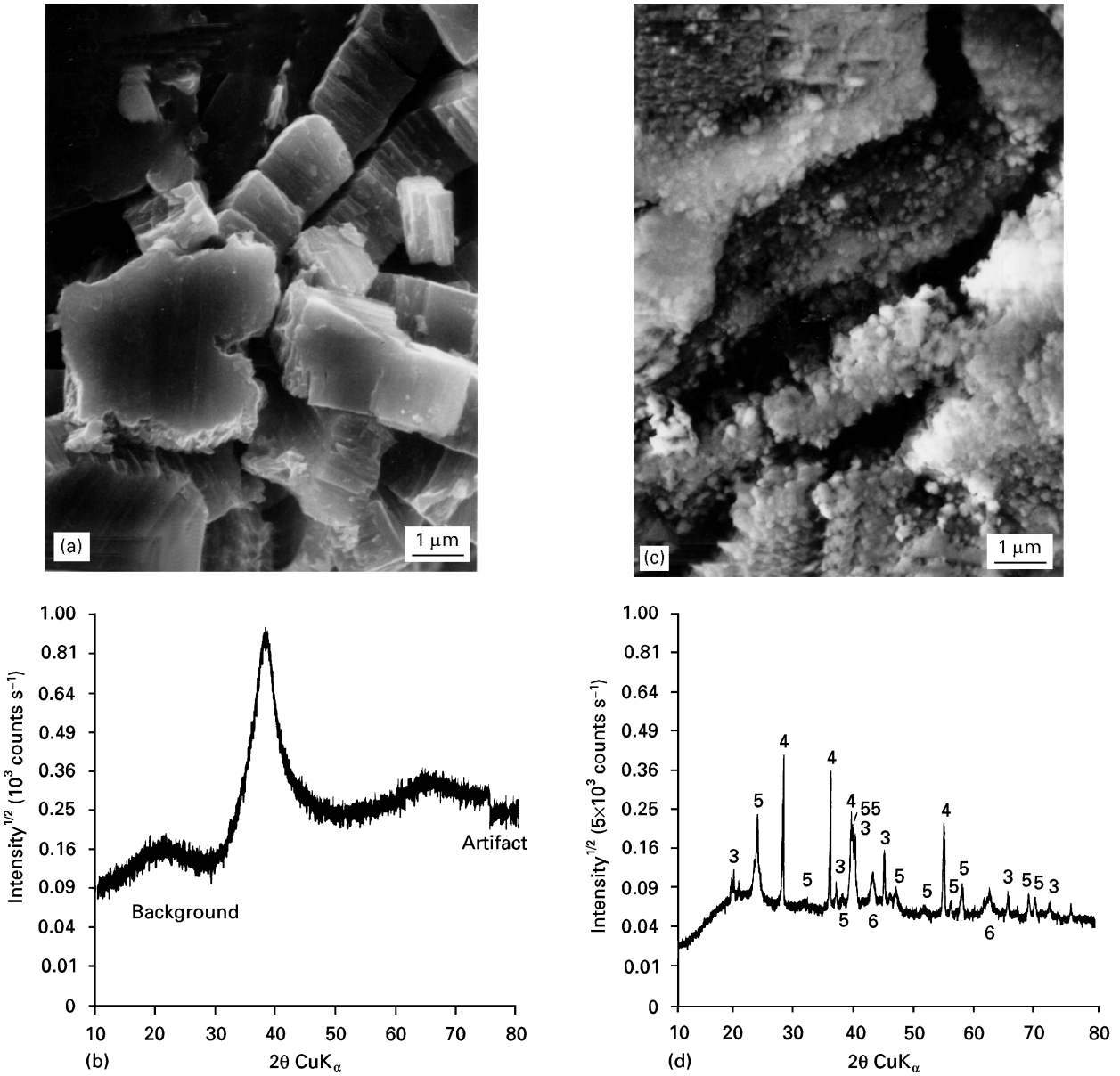

Figure 3 Microstructure and X-ray diffraction patterns of representative (a) and (b) as-prepared and (c) and (d) hydrided (350 °C and 2 MPa) magnesium–nickel prepared as amorphous thin films by co-sputtering. This particular specimen is 15 at % nickel. Key; 1, Mg; 2, Ni; 3, Mg_2Ni; 4, MgH_2; 5, Mg_2NiH_4; 6, MgO.

Magnesium with approximately 50 at % nickel, synthesized by inert-gas condensation, has a granularity of 5 to 10 nm, as seen in Fig. 2a. Application of the Scherrer formula to the X-ray diffraction line widths yields an average size of 1 nm, assuming the particles are crystalline. The pattern is more consistent with the amorphous materials than with any crystalline magnesium–nickel alloy pattern. However, it may be that these nanoscale magnesium–nickel particles are amorphous. After hydriding, as shown in Fig. 2c, two types of microstructures are evident. To the left of Fig. 2c, there are nanocrystalline particles with sizes of 10 to 20 nm, while to the right are large agglomerations of nanoscale particles. No difference in composition between the two formations is evidence by energy dispersive spectrometry. The X-ray diffraction pattern of Fig. 2d is consistent with a mixture of Mg_2Ni, $MgNi_2$, Mg_2NiH_4, and MgO. A large MgO signal is present, indicating the material is substantially oxidized.

Fig. 3 shows the microstructures and X-ray patterns for one of the magnesium–nickel thin films, with nickel concentration of 15 at %. All of the films with other nickel concentrations are similar in microstructure, and all have similar X-ray patterns except for the relative proportions of the various phases present. The synthesis method produces a compact of small broken flakes of columnar thin film, as shown in Fig. 3a. That the materials are amorphous as-deposited is clear in Fig. 3b. The very broad peaks do not match any possible particle-size broadened crystalline phases. All compositions tested, 15, 33, 60 and 85 at % Ni, were amorphous as-deposited with the same diffraction pattern. Pure Mg and pure Ni films were of course crystalline. After hydriding, some remnants of the overall flake microstructure remain, but the flakes have disintegrated into agglomerations of submicron particles, typically 500 nm diameter. The X-ray pattern shows that the initially amorphous films crystallized after hydriding. The hydrides MgH_2 and

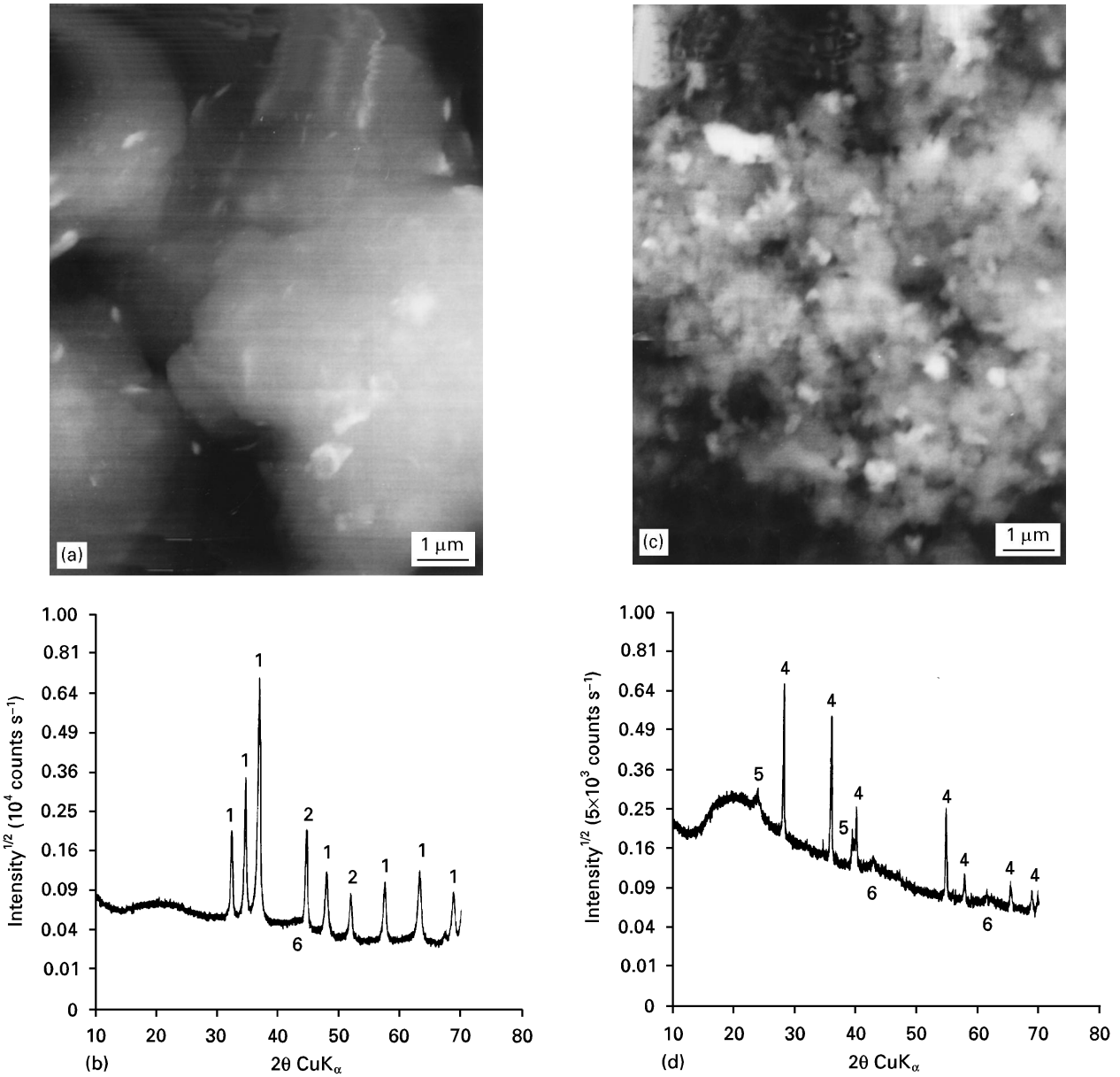

Figure 4 Microstructure and X-ray diffraction patterns of representative (a) and (b) as-prepared and (c) and (d) hydrided (350 °C and 2MPa) magnesium–nickel prepared by ball milling. This specimen is 10 at % nickel. Key; 1, Mg; 2, Ni; 3, Mg_2Ni; 4, MgH_2; 5, Mg_2NiH_4; 6, MgO.

Mg_2NiH_4, some unhydrided Mg_2Ni, and small amounts of MgO are present. MgO is more prevalent for the higher magnesium concentrations, while for higher nickel contents unreacted Mg_2Ni and $MgNi_2$ are more prevalent.

Ball-milled magnesium–nickel with 10 at % Ni is shown in Fig. 4. As milled, the material consists of large blobs of magnesium with dispersed submicron nickel particles. The X-ray pattern shows elemental crystalline magnesium and nickel, and a trace of MgO, but no magnesium–nickel compounds. In particular, the equilibrium phase expected in this region, Mg_2Ni, is not in evidence. Slightly more Mg_2Ni is present in specimens with 20 and 30 at % nickel, but all of the specimens are predominantly composites of magnesium and submicron nickel particles. Clearly, the 50 h milling time is sufficient to refine the grain sizes but does not produce complete mechanical alloying. As will be seen below, however, full alloying of the nickel and magnesium is not necessary to achieve good hydriding characteristics.

4. Hydrogen capacity

The hydrogen capacities of the thin film and ball-milled materials are shown in Fig. 5. The solid line indicates the theoretical maximum hydrogen content assuming ideal stoichiometry of equilibrium hydride phases MgH_2, Mg_2NiH_4 and Ni_2H. These data represent the hydrogen content measured in hydrogen exposure increments of about 4 h.

A series of measurements were made on the same sample as a function of hydride–dehydride cycle, and that accounts for the vertical distribution of data at each concentration. In general, the hydrogen content increased with increasing number of cycles. This activation effect was most pronounced for the thin film materials, and this will be more apparent in the next

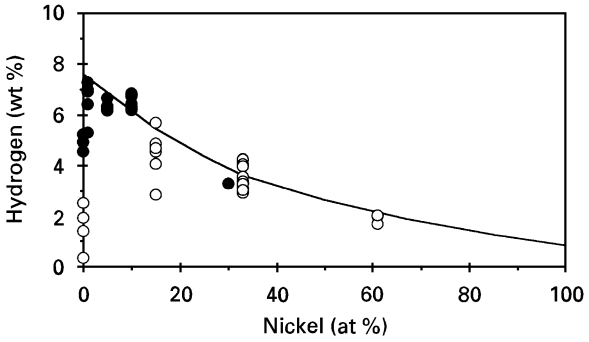

Figure 5 Hydrogen capacity of the magnesium–nickel alloys prepared by the thin film codeposition and ball-milling methods. The specimens prepared by inert gas condensation were too small to measure the total hydrogen capacity. Key: ○ thin films; ● ball milled; —— theoretical.

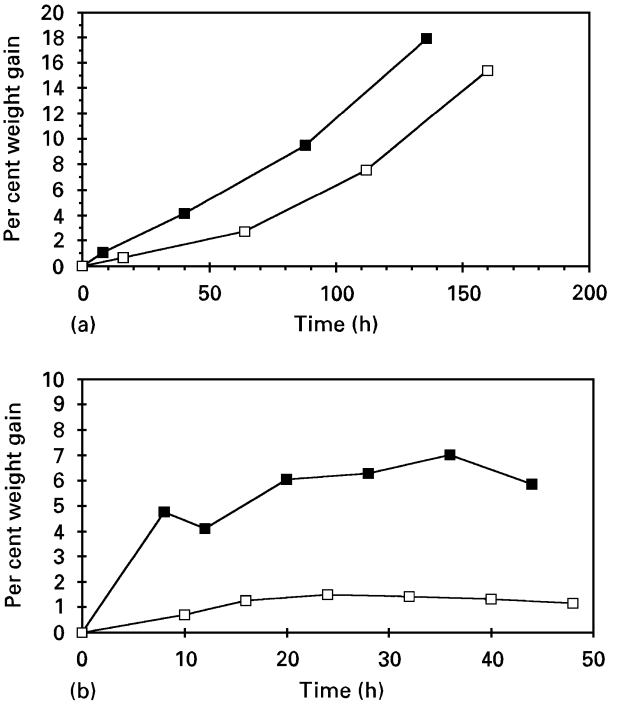

Figure 6 Weight changes upon hydride–dehydride cycling of (a) the pure magnesium and (b) a 15% magnesium–nickel thin film, showing both reversible hydride/dehydride and irreversible oxidation weight changes. Note that the 15% nickel specimen stabilizes eventually, but only after a series of cycles over a 20 h period, while the pure magnesium continues to exhibit irreversible behaviour.

section. The ball-milled materials did not show significant activation behaviour after the first hydriding cycle.

The key results indicated by this graph are that, except for pure magnesium, the ball-milled alloys were capable of attaining nearly the theoretical maximum hydrogen capacity within the nominal 4 h hydrogen exposure times without an activation cycle. The thin film materials could achieve theoretical maximum capacity given enough 4 h hydride–dehydride cycles for activation. The pure magnesium in 4 h exposures never achieved more than 40% of theoretical capacity in the case of thin films, or 75% in the case of ball-milled material. From Fig. 5, it is clear that even trace amounts of nickel cause a significant improvement in hydrogen capacity.

5. Hydriding and dehydriding rates

The hydriding kinetics of the thin films were not measured directly, but some information can be qualitatively inferred. Fig. 6 shows the net weight change of the specimens as a function of time corresponding to each hydride or dehydride treatment. For example, in Fig. 6a, for pure magnesium film, the first filled marker on the graph is the weight change relative to the as-synthesized weight after the first hydride treatment, and the first open marker corresponds to the weight change after the subsequent dehydride treatment. The bottom curve with the open markers indicates an irreversible weight gain as a function of time or cycle. The difference between the upper, curve with filled markers and the irreversible weight change corresponds to the reversible weight change. This is assumed to be associated with reversible hydrogen uptake. The irreversible part of the weight gain is associated with oxidation of the magnesium when the specimens were removed from the hydriding chamber to be weighed.

The important features of Fig. 6 are that, for the pure magnesium, even after over 100 h of hydride–dehydride cycling, neither the hydrogen uptake nor the oxidation has stabilized. On the other hand, for the 15 at % nickel specimen, the behaviour has stabilized (within the scatter of the data) by about 20 h cumulative treatment. Still, the curve indicates that the properties are still changing during the first 10 h, and that suggests that the hydriding kinetics of the as-deposited films are relatively slow with a characteristic time-scale of hours.

The ball-milled material, however, exhibits much faster kinetic behaviour. Fig. 7 shows the pressure changes as a function of time during dehydrogenation of a pure magnesium specimen and one with 5 at % nickel. The heating rates were the same in both cases. The magnesium–5 at % nickel specimen released about 30% of its hydrogen within 20 min and achieved almost 90% of its final pressure within an hour. The pure magnesium took at least 3 h to achieve 90% release, releasing virtually no hydrogen at all within the first hour. In other words, the figure indicates that the 5 at % nickel material releases at least 10 to 20 times more hydrogen than pure magnesium per gram of alloy, for release times of less than 1 h. This is compounded by the fact that the net capacity, from Fig. 5, is substantially higher for the alloy than for pure magnesium.

Interpretation of the data of Fig. 7 is slightly complicated by the fact that the temperatures are increasing with time after the furnace is turned on. The actual specimen temperatures could not be measured for various reasons, and the temperature indicated is that of the furnace core. It is observed that the magnesium releases virtually no hydrogen during the first hour, before more rapid release takes over. It therefore could be a manifestation of a thermal activation for hydrogen desorption as the temperature reaches some critical value. It is an interesting and significant result that

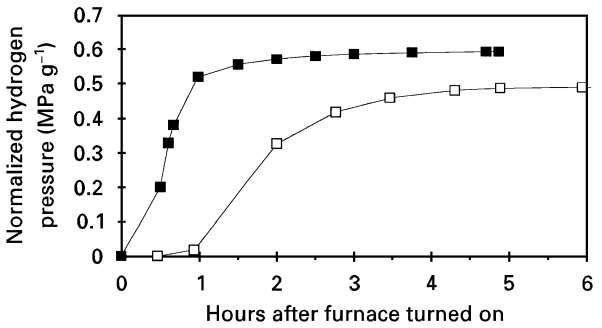

Figure 7 Pressure increase at constant volume in the reaction chamber during hydriding of pure ball-milled magnesium and magnesium with 5 at % nickel. Key: —□— pure Mg; —■— Mg–5% Ni.

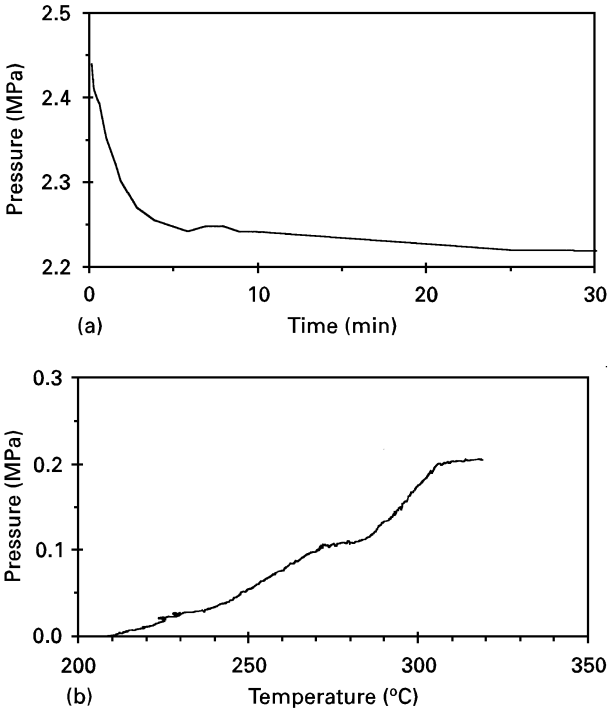

Figure 8 (a) Hydrogen uptake at 330 °C versus time and (b) dehydrogenation at 2 °C min^{-1} versus temperature of a ball-milled specimen with 30 at % nickel.

the 5% alloy did not exhibit this activation, while the pure magnesium did.

Fig. 8 shows the hydrogen uptake versus time at constant temperature and dehydrogenation versus temperature while slowly heated for a Mg–30 at % Ni specimen. In this case, the uptake, Fig. 8a, is very rapid indeed, achieving 90% of its steady state within 5 min. The desorption curve indicates a thermal activation temperature of around 270 °C, which is somewhat less than that of pure magnesium. There also is an indication of another desorption occurring at the even lower temperature of 220 °C.

6. Discussion

Superficially, the ball-milled alloys described in the present work appear similar to results reported by Song [10,11] on mechanically alloyed magnesium with low concentrations of nickel. However, there are several important differences. Specifically, the highest hydrogen capacity reported by Song is at most 4–5 wt % hydrogen, only 75% of the theoretical capacity, for alloys of about 4.5 and 12 at % Ni, and only after at least 5 hydride–dehydride cycles. Our alloys with compositions of 5 and 10 at % Ni achieved at least 6 wt % hydrogen loading on the first cycle, without requiring activation cycles. Song reports that the best hydriding characteristics in terms of both capacity and rates were achieved with Mg–12 at % Ni, while our results indicate that 5 at % Ni was optimal.

There are differences in preparation and microstructures that may account for these differences. Song processes the alloys by milling for short periods (5 min) at high energies, then relies on subsequent hydride–dehydride cycling to react nickel with magnesium to form Mg_2Ni. Particle sizes achieved appear to be in the micron range after hydriding. Our process uses long milling times, 50 h, to achieve submicron materials consisting of magnesium with embedded nanocrystalline nickel particles, with minimal Mg_2Ni phase formed. Following hydride–dehydride cycling, our particle sizes are still submicron. Furthermore, the presence of the mineral oil and the post-milling consolidation step may be key in protecting the alloy from oxide poisoning prior to hydriding.

7. Conclusions

The physical vapour deposition with inert gas condensation method, while yielding the smallest particle sizes of the highest purity, has the limitation that the process yield and production rates are very low. In addition, the nanocrystalline particles seem to be unstable against grain enlargement and agglomeration during hydriding and very prone to oxidation. The material deposited as thin films, while of higher yield and production rate, are more stable against oxidation but are characterized by slow hydriding kinetics. Of the three synthesis methods used, ball milling yields the best results in terms of both process yield and hydriding behaviour. The ball mill products in mineral oil might have aided in preventing oxidation during handling and appear to have no adverse effect on the properties.

The more significant and potentially useful result of this work is that only very low nickel concentrations in magnesium, on the order of a few per cent, are needed in ball-milled alloys to achieve three key important characteristics: optimum hydrogen capacity, significantly increased hydriding and dehydriding rates relative to magnesium, and obviating the need for activation.

Acknowledgements

The authors wish to thank Dr D. Slattery of the Florida Solar Energy Center for performing hydrogen uptake measurements on a few of our specimens early in this work. We acknowledge the contributions of Mr K. Robinson of the Physical Metallurgy Branch, Materials Science and Technology Division, Naval Research Laboratory for preparing the ball-milled

specimens, and Dr D. A. Meyn, a consultant to Geo-Centers, Inc., for performing the hydrogen capacity measurements in the Environmental Effects Branch, Materials Science and Technology Division, Naval Research Laboratory. Mr Jun Choi participated in the amorphous film specimen preparation as a Science and Engineering Apprenticeship Program (SEAP) student during the summer of 1994. R. L. Holtz of Geo-Centers, Inc., is under contract N00014-93-C-2160 to the Materials Science and Technology Division, US Naval Research Laboratory.

References

1. J. J. REILLY and R. H. WISWALL, JR, *Inorg. Chem.* **7** (1968) 2254.
2. D. L. DOUGLASS, *Metall. Trans.* **6A** (1975) 2179.
3. M. Y. SONG, E. I. IVANOV, B. DARRIET, M. PEZAT and P. HAGENMULLER, *Int. J. Hydrogen Energy* **10** (1985) 169.
4. E. IVANOV, I. KONSTANCHUK, A. STEPANOV, and V. BOLDYREV, *J. Less-Common Metals* **131** (1987) 25.
5. L. ZALUSKI, A. ZALUSKA and J. O. STROM-OLSEN, *J. Alloys Compo.* **217** (1995) 245.
6. A. K. SINGH, A. K. SINGH and O. N. SRIVASTAVA, *ibid.* **227** (1995) 63.
7. L. ZALUSKI, A. ZALUSKA, P. TESSIER, J. O. STROM-OLSEN and R. SCHULZ, *ibid.* **217** (1995) 295.
8. G. M. FRIEDLMEIER and J. C. BOLCICH, *Int. J. Hydrogen Energy* **13** (1988) 467.
9. J. C. BOLCICH, A. A. YAWNY, H. L. CORSO, H. A. PERETTI and C. O. AYALA, *ibid.* **19** (1994) 605.
10. M. Y. SONG, *ibid.* **20** (1995) 221.
11. *Idem*, *J. Mater. Sci.* **30** (1995) 1343.
12. H. IMAMURA, Y. MURATA and S. TSUCHIYA, *J. Less-Common Metals* **135** (1987) 277.
13. H. IMAMURA, Y. USUI and M. TAKASHIMA, *ibid.* **175** (1991) 171.
14. R. L. HOLTZ and V. PROVENZANO, *NanoStructured Mater.* **4** (1994) 241.
15. R. L. HOLTZ, M. A. IMAM and D. A. MEYN, in "*Synthesis/Processing of Lightweight Metallic Materials*", edited by F. H. Froes, C. Suryanarayana and C. M. Ward-Close (The Minerals, Metals and Materials Society, Warrendale, Pennsylvania, 1995) p. 339.

Received 28 May
and accepted 23 October 1996